SNAREs can promote complete fusion and hemifusion as alternative outcomes

Claudio G. Giraudo,[1] Chuan Hu,[1] Daoqi You,[3] Avram M. Slovic,[1] Eugene V. Mosharov,[2] David Sulzer,[2] Thomas J. Melia,[1] and James E. Rothman[1]

[1]Department of Physiology and Cellular Biophysics and [2]Department of Neurology, Columbia University College of Physicians and Surgeons, New York, NY 10032
[3]Memorial Sloan-Kettering Cancer Center, Long Island City, NY 11101

Using a cell fusion assay, we show here that in addition to complete fusion SNAREs also promote hemifusion as an alternative outcome. Approximately 65% of events resulted in full fusion, and the remaining 35% in hemifusion; of those, approximately two thirds were permanent and approximately one third were reversible. We predict that this relatively close balance among outcomes could be tipped by binding of regulatory proteins to the SNAREs, allowing for dynamic physiological regulation between full fusion and reversible kiss-and-run–like events.

Introduction

Cognate v- and t-SNARE on vesicles and target membrane pair to form the core machinery for intracellular membrane fusion (Sollner et al., 1993). Energy made available from the zipping-up of the SNARE complex (Sutton et al., 1998) is used to drive the fusion of lipid bilayers (Weber et al., 1998; Hu et al., 2003; Fix et al., 2004). To a remarkable degree, compartmental specificity of intracellular membrane fusion can be recapitulated from the pattern of fusion by isolated SNARE proteins (McNew et al., 2000a; Paumet et al., 2001, 2004; Parlati et al., 2002).

The "stalk hypothesis" (Chernomordik et al., 1987; Tamm et al., 2003) proposes that membrane fusion proceeds through a hemifusion intermediate before fusion pore opening. In model lipid bilayer fusion studies (Lee and Lentz, 1997), hemifusion appears to develop before inner leaflet or contents mixing, and a large variety of mutated viral fusion protein constructs give rise to a nonprogressing hemifusion endstate termed "unrestricted hemifusion" (Kemble et al., 1994; Melikyan et al., 1997, 2000; Chernomordik et al., 1998; Armstrong et al., 2000).

The exocytic fusion pores are dynamic and can "flicker" (Breckenridge and Almers, 1987; Monck and Fernandez, 1992). "Kiss and run," the partial release of vesicle contents through a transient fusion pore that rapidly recloses, has been shown in the exocytosis of both large secretory granules (Alvarez de Toledo et al., 1993) and small synaptic vesicles (Gandhi and Stevens, 2003; Staal et al., 2004). Analogous reversible fusion events have not been reported in reconstituted SNARE systems. Indeed, these types of transient events would only be observable in an experimental system that monitors individual fusion events.

Here, we expand on a cell fusion assay in which "flipped" SNAREs are ectopically expressed on the cell surface (Hu et al., 2003) to monitor single fusion events between cells. Using a range of extracellular and intracellular membrane markers, content markers, and protein constructs, we find that SNAREs can promote hemifusion events as permanent outcomes to a surprising degree.

Results

Membrane fusion outcomes by SNAREs

Previously, we demonstrated that "flipped" SNAREs, fused to signal sequences (Fig. 1 A) and expressed on the cell surface, are sufficient to fuse whole cells, evidenced by the mixing of cytosolic fluorescent proteins and even fluorescently labeled whole nuclei (Hu et al., 2003). Transient or other fusion outcomes likely would not be apparent in an assay that monitors fusion in population (Weber et al., 1998). The cell–cell assay, however, provides a picture of individual fusion events in which minority populations may be detected. Here, we describe a variety of fusion assays designed to identify cells with differential mixing of lipids and contents.

The cell–cell fusion assays we present here use various combinations of soluble and lipidic probes to simultaneously monitor content and lipid mixing between cells. To monitor lipid mixing with the cell–cell fusion assays, we took advantage

C.G. Giraudo and C. Hu contributed equally to this paper.

Correspondence to James E. Rothman: jr2269@columbia.edu

Abbreviations used in this paper: CMFDA, 5-chloromethylfluorescein diacetate; GPI, glycosylphosphatidylinositol; PI-PLC, phosphatidylinositol-specific phospholipase C; TMD, transmembrane domain.

The Journal of Cell Biology, Vol. 170, No. 2, July 18, 2005 249–260
http://www.jcb.org/cgi/doi/10.1083/jcb.200501093

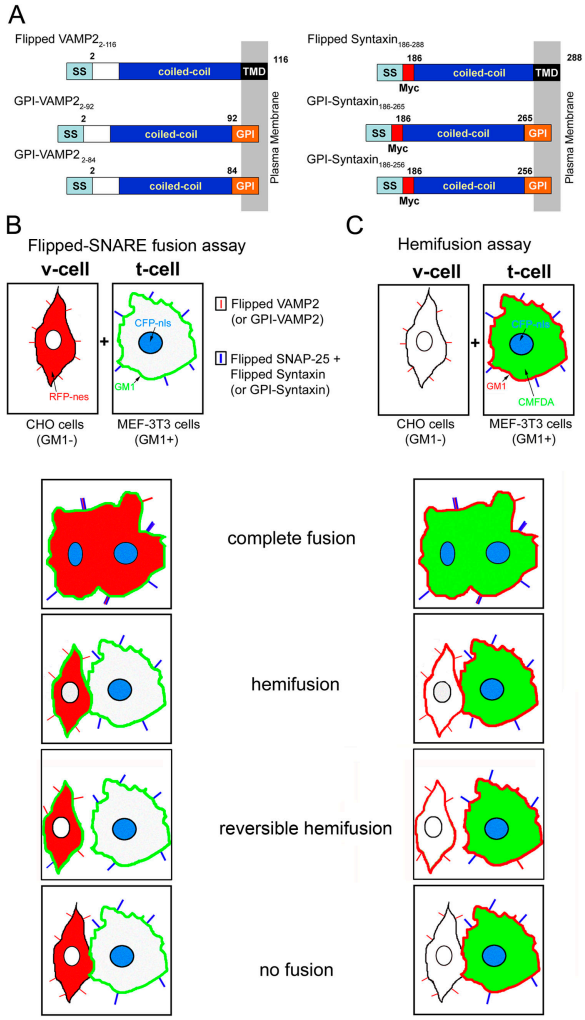

Figure 1. **Schemes of constructs used and fusion outcomes obtained with the cell–cell fusion assays.** (A) The domain structure of GPI-anchored SNAREs. The preprolactin signal sequence (SS) was fused to the NH_2 terminus of VAMP2 and the Syntaxin H3 domain. The transmembrane domains (TMD) of VAMP2 and Syntaxin were replaced with the GPI-anchoring sequence of decay-accelerating factor. A Myc tag (red) was engineered between the NH_2 terminus of the Syntaxin H3 domain and the signal sequence. Two additional GPI-anchored SNAREs (GPI-$VAMP_{2\text{-}84}$ and GPI-$Syntaxin_{186\text{-}256}$), in which amino acids 85–92 in VAMP2 and amino acids 257–265 in Syntaxin H3 were deleted, were generated to bring the coiled-coil domains closer to the membrane anchors. (B) Cell fusion assay design monitoring lipid mixing and content mixing. The cytoplasm of CHO cells (GM1 negative) that expressed flipped VAMP2 or GPI-VAMP2 was labeled with RFP-nes. The nuclei of MEF-3T3 cells (GM1 positive) that express flipped t-SNAREs or GPI-anchored t-SNAREs were labeled with CFP-nls. The t-cells were harvested with an EDTA buffer, and overlaid on the v-cells. Cells were fixed after 6 h at 37°C. GM1 was stained with FITC-cholera toxin β-subunit (green). Complete fusion resulted in cells containing red cytoplasm, cyan nuclei, and green cell surface staining. In hemifused cells, GM1 transferred from t-cells to the contacting CHO v-cells in the absence of the mixing of the cytoplasmic markers. In the event of reversible hemifusion, after GM1 is transferred from t-cells to v-cells, the v- and t-cells detached from each other. In the no fusion cells, all the markers remained within the original cells. (C) Cell fusion assay designed to detect small fusion pores using CMFDA. MEF-3T3 cells (GM1 positive) that express CFP-nls and either flipped t-SNAREs or GPI-anchored t-SNAREs were preloaded with soluble dye CMFDA, detached, and mixed with CHO v-cells (GM1 negative) expressing flipped VAMP2 or GPI-VAMP2. GM1 lipid, originally present only in the t-cell plasma membrane, was labeled with $Alexa^{594}$-cholera toxin β-subunit (red). In completely fused cells, all three markers (CFP-nls, CMFDA, and GM1) are transferred from the t-cells to the v-cells, evidenced as a cell with multiple cyan nucleus, green cytoplasm, and red plasma membrane staining. In hemifused cells, only the lipid probe GM1 is transferred to the v-cells, showing a v-cell red-labeled plasma membrane without green cytoplasm and cyan nuclei staining. Reversible hemifusion resulted in v-cells that were positive for GM1 staining but not in contact with any t-cells.

of the fact that the GM1 ganglioside is absent on the surface of CHO cells due to the lack of a key enzyme in the pathway of ganglioside biosynthesis (Rosales Fritz et al., 1997) but is present on the surface of MEF-3T3 cells (Fig. 1, B and C). The cell-specific localization of GM1 was detected through binding of fluorescently labeled cholera toxin β-subunit (FITC-ctxβ [Fig. 1 B, green] or $Alexa^{594}$-ctxβ [Fig. 1 C, red]). When MEF-3T3 cells expressing flipped t-SNAREs (GM1 positive) were mixed with CHO cells expressing flipped v-SNAREs (GM1 negative), membrane lipid mixing can be observed as the development of ctxβ-dependent fluorescence on the previously GM1-negative v-SNARE cells. By including various fluorescently labeled content markers, two assays were developed in which different potential membrane fusion outcomes could be distinguished according to different patterns of color mixing (Fig. 1, B and C).

In the original flipped SNARE fusion assay containing a lipid mixing marker (Fig. 1 B), the t-SNARE cell membrane and nuclei were labeled using green (FITC) ctxβ and the cyan fluorescent protein (bearing a nuclear localization signal; CFP-nls), respectively. The v-SNARE cell cytoplasm was labeled with the red fluorescent protein (bearing nuclear export signal; RFP-nes). Thus, complete fusion will result in the complete mixing of red cytoplasm (from the v-cells), cyan nuclei (from the t-cells), and green-ctxβ–bound GM1 (from the t-cells). Lipid mixing can be detected by the transfer of only the GM1 lipid to the v-cells, but not the cyan nuclei.

In stable cell lines expressing flipped SNAREs and the appropriate fluorescent markers (as depicted in the original flipped SNARE fusion assay Fig. 1 B) and incubated together for 6 h, complete fusion occurs in 23 ± 3% (mean ± SD) of the cells in contact (Fig. 2, arrowheads), which is consistent with our earlier observations in COS cells (Hu et al., 2003). Lipid transfer without content mixing (i.e., incomplete fusion) was observed in 14 ± 3% (Fig. 2, arrows) of contacting cells. Z-section analysis confirmed the absence of a t-cell–derived cyan-nucleus in these incompletely fused cells (unpublished data). We also observed a reversible version of the incomplete fusion; i.e., v-cells containing lipid mixing markers that are no longer in contact with a t-cell (Fig. 2, asterisks). These kiss-and-run–like cells have apparently experienced transient mixing of the lipid bilayers to become GM1 positive without significant contents mixing before physically separating. We observe one such v-cell for about every 20 contacting v- and t-cell pairs. All three observed fusion outcomes are SNARE dependent. No fusion subtype was observed if SNARE pairing is disrupted by either titrating free t-SNARE with the cytoplasmic domain of the v-SNARE (Fig. 2, control) or by expressing Syntaxin 1 alone (without SNAP-25; not depicted).

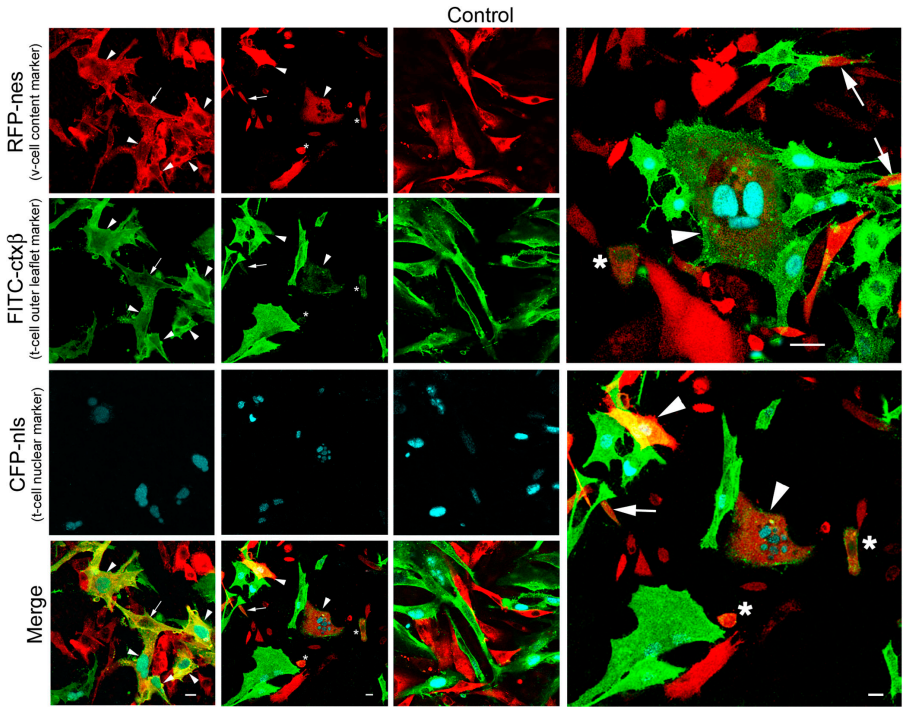

Figure 2. **Complete fusion, incomplete fusion, and reversible incomplete fusion by flipped SNAREs.** As described in Fig. 1 B, CHO stable v-cells expressing flipped VAMP2 and RFP-nes were detached and overlaid on MEF-3T3 cells expressing flipped Syntaxin, flipped SNAP-25, and CFP-nls. The cells were fixed after 6 h at 37°C. GM1 was stained with FITC-cholera toxin β-subunit (green). Arrowheads indicate fused cells, arrows indicate incomplete fused cells, and asterisks indicate reversible incomplete fusion. (Control) The cytoplasmic domain of VAMP2 (20 μM) completely inhibited complete fusion, incomplete fusion, and reversible incomplete fusion mediated by flipped SNAREs. Bars, 10 μm.

Incomplete fusion phenotype corresponds to hemifusion events

To further characterize the novel incomplete fusion phenotypes, we developed the hemifusion assay (Fig. 1 C) in which a smaller fluorescent probe (5-chloromethylfluorescein diacetate [CMFDA]) was used as a content marker. This modification would allow us to detect small nonenlarging fusion pores that might be missed with the original flipped SNARE fusion assay (Fig. 1 B) due to diffusional restriction of the bulky red fluorescent protein through these fusion pores. Furthermore, in this assay, all the fluorescent markers (green CMFDA as soluble content marker, CFP-nls as nuclear marker, and red Alexa^{594}-ctxβ as membrane marker) are initially limited to the t-SNARE cell to clearly identify which fluorophore is able to diffuse to v-SNARE cells. Transfer of GM1 alone to a v-cell gives the striking result of a red-bordered cell with no fluorescent content (Fig. 3, arrows), which is indicative of incomplete fusion. This transfer of red fluorescence to the unstained v-SNARE population does not occur when mock-transfected cells are used instead of v-cells (Fig. 3, right column), confirming the SNARE dependence of the assay and the lack of free exchange of the GM1 lipid. In this assay, full fusion is indicated by the presence of multiple cyan nuclei in cells containing both green CMFDA and the red ctxβ markers. Quantitative analysis of these experiments gave rise to practically the same fusion phenotype ratios (complete fusion/incomplete fusion/reversible incomplete fusion, 6.5:2.5:1) observed with the original flipped SNARE fusion assay. Moreover, with this cell fusion assay we were able to identify a fourth kind of phenotype compatible with the classic kiss-and-run process; i.e., v-cells no longer in contact with t-cells that exchanged both lipids and contents but without having cyan nuclei. Unlike the reversible incomplete fusion, the classic kiss-and-run phenotype was observed only in 2 ± 1%. Because this value is not statistically significant, further characterization will be required to determine whether this phenotype is another outcome of the SNARE-mediated fusion. Labeling the v-cell cytoplasm with CMFDA instead of the t-cell cytoplasm did not change the final proportion of fusion outcomes (unpublished data). Thus, neither big (RFP-nes) nor small (CMFDA) soluble contents markers were able to diffuse between incomplete fused. These results are in line with previous studies with viral fusion proteins in which the hemifusion phenotype has been identified as an incomplete fusion event, where lipid mixing but not content mixing is observed (Kemble et al., 1994; Melikyan et al., 1997, 2000; Cohen and Melikyan, 1998). Therefore, the SNARE-mediated incomplete fusion phenotypes observed in our cell fusion assays most likely represent hemifusion events.

Hemifusion as an outcome

Time course experiments (Fig. 4) using the original flipped SNARE fusion assay showed that hemifusion events accumulated slightly faster than complete fusion events and reached a plateau at 6 h, whereas complete fusion events continued to increase through 24 h. Eventually, all three populations settle into a plateau distribution in which complete fusion makes up ~64% of the total events, permanent hemifusion comprises 27%, and reversible hemifusion events represent 9%. The apparent stability of this distribution implies that hemifusion by SNAREs is an alternative outcome, similar perhaps to the "unrestricted hemifusion" described for some hemagglutinin viral constructs (Kemble et al., 1994; Melikyan et al., 1997, 2000; Chernomordik et al., 1998). Thus, the hemifusion we observe does not appear to be an on-pathway intermediate to full fusion. However, we cannot rule out the existence of "restricted hemifusion," the purported on-pathway intermediate inferred from chemical trapping of fusion products in various viral sys-

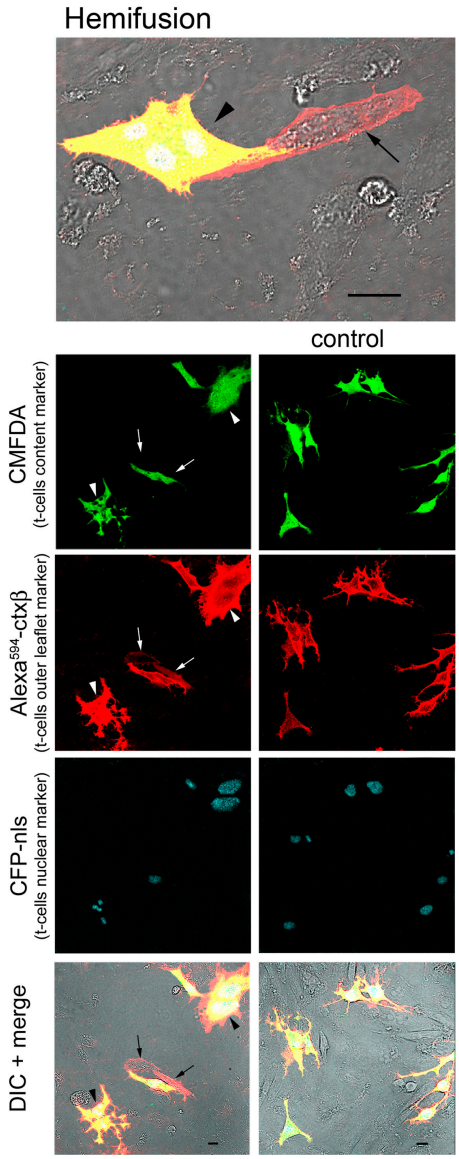

Figure 3. **Hemifusion mediated by flipped SNAREs.** As described in Fig. 1 C, MEF-3T3 stable cells expressing flipped Syntaxin, flipped SNAP-25, and CFP-nls were preloaded with CMFDA as a fluid phase marker, detached, and then seeded on a coverslip that already contained CHO stable cells expressing flipped VAMP2. Cells were fixed after 6 h at 37°C and stained with Alexa^{594}-cholera toxin β-subunit (red). Arrowheads indicate fused cells and arrows indicate hemifused cells. (top) A fused cell in contact with a hemifused one. (control) No fusion or hemifusion was observed using CHO cells that were mock transfected. Bars, 10 μm.

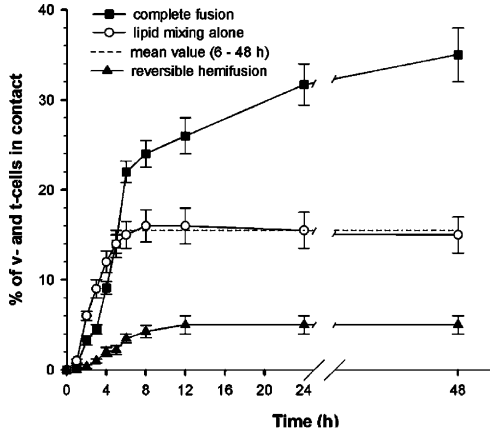

Figure 4. **Time course of complete fusion, hemifusion, and reversible hemifusion mediated by flipped SNAREs.** CHO stable v-cells were mixed with MEF-3T3 stable t-cells. At different time points, the percentage of v- and t-cells in contact that underwent complete fusion or hemifusion was determined using the assay described in Fig. 1 B. Images in 50 random fields were used for calculation of each time point. Reversible hemifusion events were calculated as a fraction of the number of v-cells in contact with t-cells. Values are mean ± SD of three independent experiments. Dashed line is the mean value from 6 to 48 h showing that the hemifusion curve reached a plateau.

tems, because the kinetic of our cell fusion assays is limited by the time required by cells to attach to the substrate and to interact to each other. This limitation may be responsible for the slower kinetic of fusion observed with a cell-based assay compared with normal SNARE-mediated fusion events.

The SNARE cytoplasmic domain with a lipid anchor is sufficient for hemifusion but not for fusion

When the transmembrane domain (TMD) of viral fusion protein hemagglutinin is replaced with glycosylphosphatidylinositol (GPI), a lipid anchor that spans only the outer leaflet of the membrane, membrane fusion ends in a hemifusion state where the outer monolayers of the membranes are fused while the inner monolayers and the aqueous contents remain segregated (Kemble et al., 1994; Melikyan et al., 1995b, 2000), establishing the central role of the HA TMD in completion of full fusion. Similarly, replacement of the TMD of SNARE proteins by lipid anchors that span a single leaflet of the bilayer inhibited complete fusion in vitro (McNew et al., 2000b; Rohde et al., 2003) and in vivo (Grote et al., 2000). To further test the role of the SNARE TMD in fusion and lipid mixing, we replaced the native TMDs of flipped VAMP2$_{2\text{-}116}$ and flipped Syntaxin 1 with the GPI-anchoring sequence of decay-accelerating factor (Fig. 1 A) to generate GPI-VAMP2$_{2\text{-}92}$ and GPI-Syntaxin$_{186\text{-}265}$. When transfected, the GPI-anchored v- and t-SNAREs were expressed on the cell surface (Fig. 5). COS cells coexpressing GPI-VAMP$_{2\text{-}92}$ and EGFP were incubated with soluble cognate t-SNAREs, consisting of the recombinant cytoplasmic domain of Syntaxin 1 complexed with full-length SNAP-25. In the confluent cell layer, soluble t-SNAREs only bound to the cells that expressed GPI-VAMP2 (Fig. 5 A, left, green cells), but not to the cells that were not transfected (Fig. 5 A, left, nonfluorescent cells), indicating that GPI-VAMP2 proteins were expressed on the cell surface and could bind t-SNAREs. Phosphatidylinositol-specific phospholipase C (PI-PLC) specifically cleaves the GPI linkage. When PI-PLC was present in the medium, little t-SNARE binding was observed (Fig. 5 A, right), confirming that GPI-VAMP2 proteins were anchored to the cell surface via GPI linkage. When COS cells were cotransfected with GPI-Syntaxin$_{186\text{-}265}$ and flipped SNAP-25/T79A,N188A, which does not contain a TMD, both proteins were expressed on the cell surface (Fig. 5 B, top). Similar to flipped t-SNAREs (Hu et al., 2003), a considerable amount of

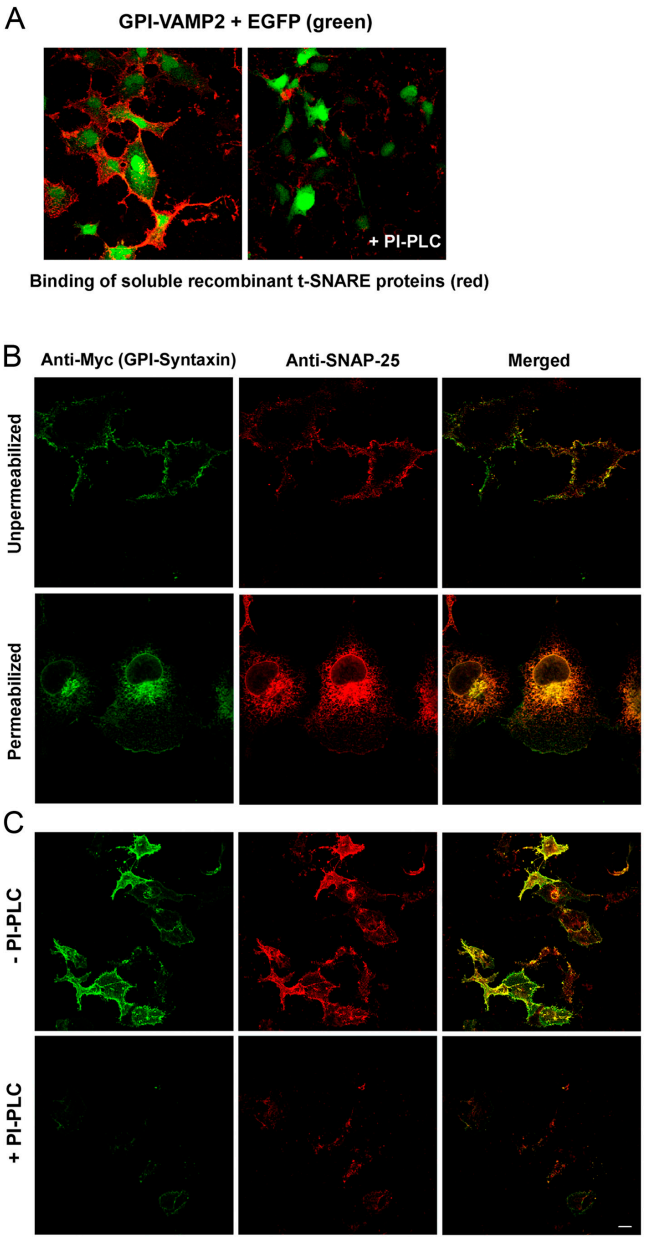

Figure 5. **Cell surface expression of GPI-anchored SNAREs.** (A) Soluble t-SNAREs bind to GPI-VAMP2. COS cells were transfected with an IRES plasmid that encodes GPI-VAMP$_{2\text{-}92}$ and enhanced GFP (EGFP). The cells were incubated with a soluble t-SNARE complex (5 μM) for 1 h at 37°C. Surface-bound t-SNARE was detected with an antibody to Syntaxin (red, merged with EGFP fluorescence). (right) When phosphatidylinositol-specific phospholipase C (PI-PLC) was included in the binding assay, little t-SNARE binding was observed. (B) Expression of GPI-anchored t-SNAREs on the cell surface. COS cells cotransfected with GPI-Syntaxin$_{186\text{-}265}$ and flipped SNAP-25 were stained with antibody to c-myc (Syntaxin, green) and antibody to SNAP-25 (red). Top, unpermeabilized cells; bottom, permeabilized cells. (C) Release of GPI-anchored t-SNAREs from the cell surface by PI-PLC. COS cells expressing Syntaxin$_{186\text{-}265}$ and flipped SNAP-25 were incubated with PI-PLC (100 mU/ml), and then stained with antibody to c-myc (Syntaxin, green) and antibody to SNAP-25 (red). Bar, 10 μm.

Syntaxin$_{186\text{-}265}$ and flipped SNAP-25 proteins reached the cell surface, although the majority of the GPI-anchored t-SNAREs remained inside the cells, probably retained by the ER quality control system (Fig. 5 B, bottom). Flipped SNAP-25 was anchored to the cell surface by forming a complex with Syntaxin$_{186\text{-}265}$. As expected, when the COS cells were treated with PI-PLC, both GPI-Syntaxin and flipped SNAP-25 proteins were released from the cell surface (Fig. 5 C).

The GPI-anchored SNAREs were defective in membrane fusion (Fig. 6). When CHO stable cell lines expressing GPI-VAMP2 were mixed with MEF-3T3 stable cells expressing GPI-Syntaxin and flipped SNAP-25, only rare complete cell fusion events were observed, at a frequency at or below the spontaneous fusion rate of negative SNARE-independent control (Fig. 6, A and B). Addition of the Vc-peptide, which prestructures the t-SNARE and accelerates membrane fusion of flipped SNAREs (Melia et al., 2002; Hu et al., 2003), did not change the outcome (Fig. 6 B).

Lipid mixing, but not content mixing, of GPI-expressing cells was observed using both original flipped SNARE fusion assay (Fig. 6 A, left, arrows) and hemifusion assay (Fig. 6 A, right, arrows), indicating that GPI-anchored SNAREs promote hemifusion. Lipid mixing was SNARE dependent, as only background activity was observed when flipped SNAP-25 was not expressed in the t-cells (Fig. 6 B), when GPI-VAMP2 was not expressed in the v-cells (Fig. 6 A, last column), or when the cytoplasmic domain of VAMP2 was added to titrate the GPI-t-SNAREs on the surface of t-cells (Fig. 6 B). SNAREs with GPI lipid anchors promoted hemifusion efficiently: 24% of the v-cells and t-cells in contact hemifused within 6 h (Fig. 6 B). Vc-peptide modestly increased hemifusion to 28% of cognate cells in contact (Fig. 6 B).

Between the SNARE domain and the TMD of both Syntaxin and VAMP2 lies a highly basic linker region that has been shown to be partially embedded within the outer leaflet of the bilayer (Kweon et al., 2003). To explore whether these membrane-proximal amino acids influence the development of hemifusion, we generated two additional GPI-anchored VAMP2 and Syntaxin 1 constructs (GPI-VAMP$_{2\text{-}84}$ and GPI-Syntaxin$_{186\text{-}256}$), which bring the coiled-coil SNARE domains closer to the GPI membrane anchor (Fig. 1 A). Similar hemifusion activity was observed when using either GPI-VAMP$_{2\text{-}92}$ or GPI-VAMP$_{2\text{-}84}$ in the v-cells or when using either GPI-Syntaxin$_{186\text{-}265}$ or GPI-Syntaxin$_{186\text{-}256}$ in the t-cells (Table I). Thus, neither the TMD nor the membrane-embedded linker is necessary to promote hemifusion of SNARE-expressing cells.

Size barriers for diffusion during hemifusion

We explored the structural boundaries imposed by hemifusion with both the flipped SNAREs and the GPI-anchored SNAREs. Hemifusion does not involve the mixing of the inner monolayers of the membranes or of soluble content. Not surprisingly, when v-cells were labeled with inner monolayer probes (EGFP with a farnesylation sequence [EGFP-f]; EYFP with a palmitoylation sequence [EYFP-pal]; or even the much smaller HA epitope fused to a farnesylation sequence) and mixed with t-cells, no transfer of the inner monolayer probes was observed in the hemifused cells (Fig. 7 A, top; and Fig. 7 B). To further determine if during hemifusion small and/or transient fusion pores open that could allow the selective passage of smaller molecules

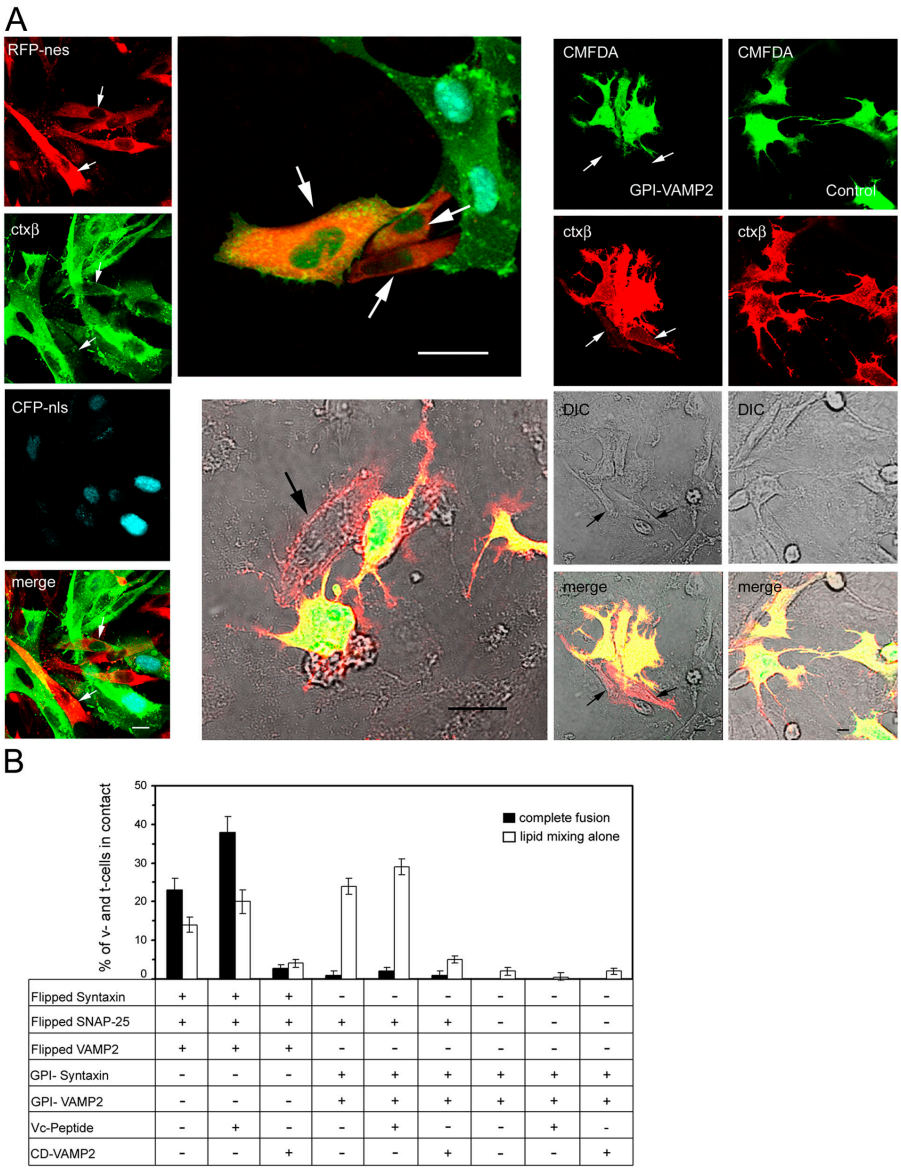

Figure 6. **GPI-anchored SNAREs promote hemifusion.** (A) MEF-3T3 cells expressing GPI-Syntaxin and flipped SNAP-25 were overlaid on CHO cells expressing GPI-VAMP2. First column, hemifusion detected with the assay described in Fig. 1 B. (third column) Hemifusion detected with the assay described in Fig. 1C. (fourth column) No hemifusion was observed when GPI-VAMP2 was not expressed in the CHO cells. Arrows point to hemifused cells. (B) The percentage of v- and t-cells in contact that underwent complete fusion or hemifusion in the presence of different combinations of flipped or GPI anchored SNAREs. Hemifusion was also detected in cell fusion mediated by flipped SNAREs. Vc-Peptide (60 μM) produced a slight increase in hemifusion mediated by GPI-anchored SNAREs, whereas the cytoplasmic domain of VAMP2 (CD-VAMP2; 20 μM) inhibited it. Filled bars, fused cells; open bars, hemifused cells. Values are mean ± SD of four independent experiments; n = 200 cells. Bars, 10 μm.

as it was observed for the hemagglutinin protein mediated fusion (Zimmerberg et al., 1994), in addition to CMFDA, we preloaded v-cells with other small (MW ~500) soluble probes; e.g., Calcein AM, 4-chloromethyl-6,8-difluoro7-hydroxycoumarin (blue CMF_2HC), and cell tracker red CMTPX. Although the transfer of GM1 was detected in the hemifused cells, no transfer of the small soluble probes was detected (Fig. 7, A and B). However, due to the limitation of the assay for detecting low level of dye transfer between cells, we cannot rule out the possibility that very small and/or transient fusion pores that do not enlarge might be forming, as it was documented for HA viral protein-mediated membrane fusion (Zimmerberg et al., 1994; Melikyan et al., 1995a; Razinkov et al., 1999).

There was a size barrier for the diffusion of molecules in the outer monolayers of hemifused cells. EYFP proteins (239 amino acids) with a GPI-anchor (GPI-EYFP) could not diffuse from v-cells to t-cells (Fig. 7 B), whereas the six amino acid epitope AU1 (DTYRYI) (GPI-AU1) transferred from the hemifused v- and t-cells nearly as efficiently as GM1 (Fig. 7 B).

Hemifused cells do not show electrically active connecting fusion pores

Although we tested a variety of membrane and fluid phase markers with different molecular weight, charge, and diameter in our cell–cell fusion assay, we considered the possibility that these tracers might be hindered from traversing small fusion pores connecting the hemifused cells that would nevertheless have conductivity. For this reason, we extended our search for very small fusion pores by performing time resolved capacitance and conductance measurements using a whole cell patch configuration. This powerful technique has both the time resolution and sensitivity required to identify even short-lived reversible pores (Zimmerberg et al., 1994; Melikyan et al., 1995a; for review see Lindau and Almers, 1995). For these experiments, we used cells expressing the original flipped SNAREs (with complete transmembrane domains). We reasoned that because these cells show a high propensity for full fusion, they may also form small pores in the apparent "hemifusion state." We chose these cells over GPI-SNARE cells because it is most probable that they produce a

Table I. **Efficiency of cell fusion and lipid mixing between different combinations of v- and t-cells**

v-SNARE cell	t-SNARE cell			
	Flipped Syntaxin 1 with flipped SNAP-25	**GPI-Syntaxin$_{186-265}$ with flipped SNAP-25**	**GPI-Syntaxin$_{186-256}$ with flipped SNAP-25**	**GPI-Syntaxin$_{186-256}$**
Flipped VAMP2	F = 23 ± 3% LM =14 ± 3%	F = 1 ± 1% LM = 18 ± 3%	F = 2 ± 1% LM = 16 ± 3%	F = 0% LM = 2 ± 1%
GPI-VAMP 2$_{2-92}$	F = 1 ± 1% LM = 17 ± 2%	F = 2 ± 1% LM = 24 ± 3%	F = 1 ± 1% LM = 22 ± 3%	F = 0% LM = 2 ± 2%
GPI-VAMP2$_{2-84}$	F = 2 ± 1% LM = 15 ± 3%	F = 1 ± 1% LM = 22 ± 4%	F = 1 ± 2% LM = 20 ± 3%	F = 0% LM = 1 ± 1%
Mock transfected	F = 0% LM = 1 ± 1%	F = 0% LM = 1 ± 1%	F = 0% LM = 1 ± 1%	F = 0% LM = 0%

The percentage of v-cells expressing either flipped VAMP2, GPI-VAMP2$_{2-92}$, or GPI-VAMP2$_{2-84}$ and t-cells expressing either flipped Syntaxin, GPI-Syntaxin$_{186-265}$, or GPI-Syntaxin$_{186-256}$ with or without flipped SNAP-25 in contact that underwent complete fusion (F) or lipid mixing alone (LM) were determined using the assay described in Fig. 1 B. Values are the mean ± SD of three independent experiments (n = 200).

detectable fusion pore. After 24-h incubation, cells were stained with FITC-ctxβ and cell membrane capacitances of single non-fused, fully fused, and hemifused CHO cells were determined (Fig. 8, A and B; and see Materials and methods). Single CHO cells, which are typically smaller than 3T3 fibroblasts, had membrane capacitances in the range of ~13–15 pF, corresponding to a surface area of 1170–1350 μm^2 (Fig. 8 C), whereas 3T3 cells exhibited capacitances of 18–32 pF (1620–2880 μm^2; not depicted) assuming a membrane-specific capacitance of 9 fF/μm^2 (Albillos et al., 1997). When hemifused cells were patched, whole cell recordings yielded capacitance measurements consistent with single cells, suggesting that there was no electrical continuity between the contents of the cells to a resolution of 100 ms (Nyquist frequency) given a sampling frequency of 20 Hz. In contrast, the membrane capacitance of fully fused cells was significantly higher, consistent with the visually observed much larger size of these cells compared with single or hemifused cells (Fig. 2).

To confirm that there were no pore fluctuations during the time course of the experiment, we measured the changes in the whole cell current in patched CHO hemifused cells to a resolution of 100 μs (Nyquist frequency), taking advantage of the high frequency of the ITC-18 A/D converter, which is 20 kHz. This temporal resolution is the lower limit at which we might expect to observe even the very fast flickers associated with dopamine exocytosis from rat cultured ventral midbrain neurons (Staal et al., 2004). No steplike changes in the steady-state current (I_{ss}) were observed during the time course of the experiments, although a slight drift of the current was sometimes observed (Fig. 8 D), yet in

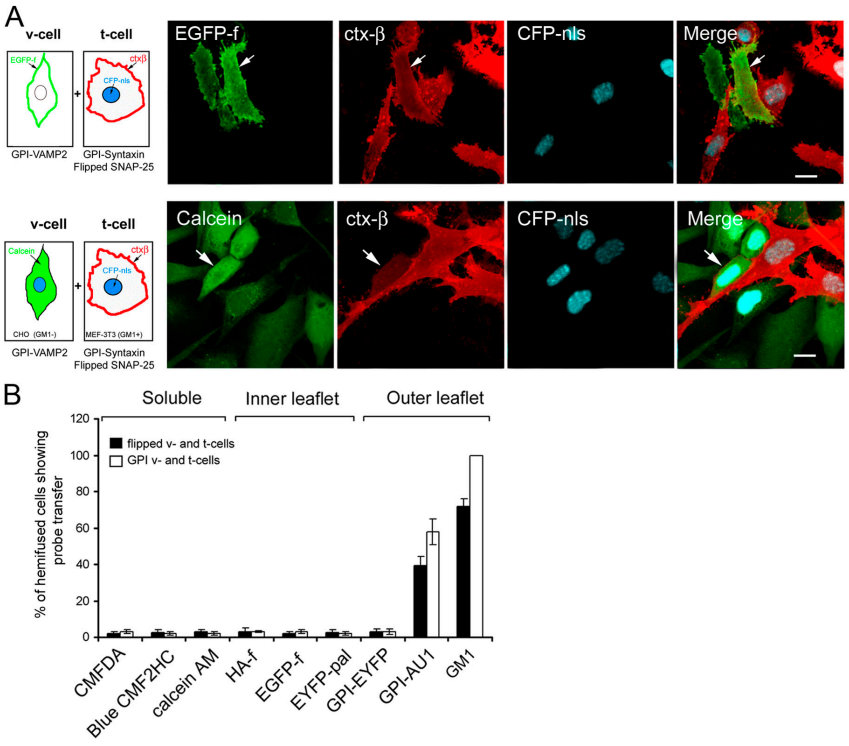

Figure 7. **Hemifusion does not involve the mixing of the inner monolayers of the membranes or of soluble content.** (A) CHO cells transiently transfected with GPI-VAMP2 and EGFP-f were detached and incubated with the MEF 3T3 t-cells (top). GM1 was detected with Alexa^{594}-ctxβ (red). No transfer of EGFP-f was observed in the hemifused cells. CHO v-cells that were transiently transfected with GPI-VAMP2 and CFP-nls were preloaded with the cytoplasmic dye Calcein AM (green), and then detached and incubated with MEF-3T3 t-cells that expressed CFP-nls, GPI-Syntaxin, and flipped SNAP-25 (bottom). The cells were fixed after 6 h and stained with Alexa^{594}-ctxβ (red). Arrows indicate hemifused cells. Transfer of GM1, but not Calcein AM, was observed in the hemifused cells. Bars, 10 μm. (B) Summary of results using different types of probes. 5-Chloromethylfluorescein diacetate (CMFDA), Calcein AM, and 4-chloromethyl-6,8-difluoro7-hydroxycoumarin (Blue CMF$_2$HC) are small soluble dyes; EFGP-f, EYFP bearing a palmitoylation sequence (EYFP-pal), and HA epitope fused to a farnesylation sequence (HA-f) labeled the inner leaflet of the plasma membrane; GPI-anchored EYFP (GPI-EYFP), GPI-anchored epitope AU1 (GPI-AU1), and ctxβ labeled the outer monolayer of the plasma membrane. Filled bars, percentage of hemifused cells showing probe transfer mediated by flipped SNAREs; open bars, percentage of hemifused cells showing probe transfer mediated by GPI-anchored SNAREs. Only GPI-AU1 and GM1 were transferred in the hemifused cells. Values are mean ± SD of two independent experiments; n = 100 cells.

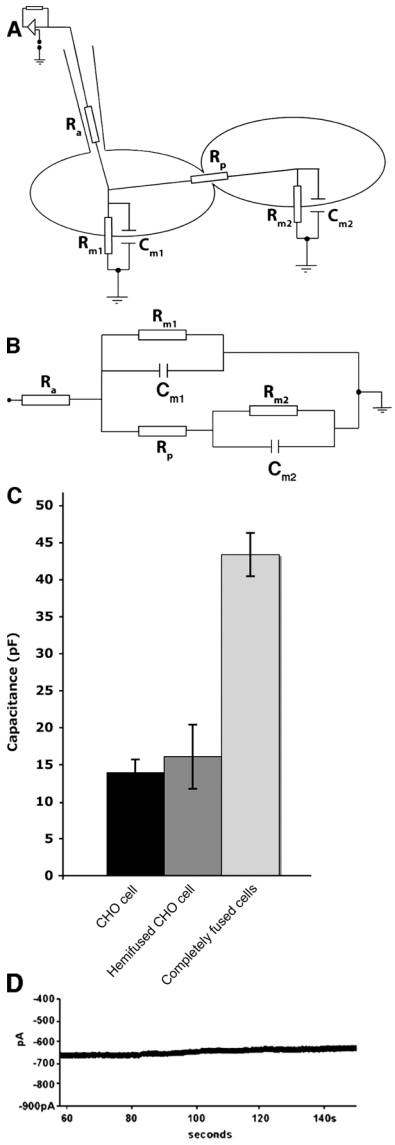

Figure 8. **Hemifused cells do not show electrically active connecting fusion pores.** Electrical diagram (A) and equivalent circuit (B) of hemifused cells in the whole cell configuration. R_a is the access resistance, R_{m1} and R_{m2} are the resistances of cells 1 and 2, respectively, C_{m1} and C_{m2} are the membrane capacitances of cells 1 and 2, respectively, and R_p is the resistance of a theoretical pore connecting the two cells. (C) Cell capacitances ± SD averaged over 100 s of recording. A 20-Hz sampling frequency (see Materials and methods) was used. Measurements of single CHO cells ($n = 3$) as well as hemifused cells patched from the CHO cell ($n = 3$) and cell capacitance of completely fused cells are shown ($n = 3$). Hemifused cells appear to have capacitances similar to single cells, whereas fused cells have membrane capacitances equal to the sum of one CHO and 3T3 cell. (D) A representative recording of cell resistance ($n = 4$) taken over 100 s. A 20-kHz sampling frequency was used. Pore opening would be observed as a downward current step.

the opposite direction expected if a fusion pore were to open. We then attempted to set a limit on fusion pore resistances that might escape detection in our setup. We estimated the ratio of the whole cell currents before and after the fusion of two identical cells:

$$\frac{I_{ss}(2cells)}{I_{ss}(1cell)} = \frac{2R_m + R_p}{R_m + R_p};$$

where R_m is the membrane resistance of the cell (see Materials and Methods). Assuming $R_m = 600$ MΩ, this relationship predicts that a 10% increase in I_{ss} (which would be easily observed in our experiments) would correspond to a pore resistance (R_p) of 5 GΩ or a fusion pore diameter of ∼2 nm (Hille, 1984), using a thickness of 15 nm for hemifused membrane (Monck and Fernandez, 1992). We cannot rule out the possibility of a constitutively open micro fusion pore (a pore that formed before we patched on the cell and remained stable throughout the experiment). However, our experimental resolution was at the lower limit described for pore flickering in synaptic vesicles (∼100 μs; Staal et al., 2004), and therefore a flickering event in our hemifused cells would likely have been detected. Therefore, we conclude that if dynamic pores were forming, their lifetimes would be ≤100 μs and their sum resistances would exceed 5 GΩ (indicating a pore diameter <2 nm).

Discussion

Bilayer membrane fusion models (Chernomordik et al., 1987; Lee and Lentz, 1997; Tamm et al., 2003) propose that membrane fusion proceeds through a hemifusion intermediate before fusion pore opening. A large number of studies with lipid bilayers and viral fusion assays have identified the existence of a nonprogressing hemifusion endstate termed "unrestricted hemifusion" (Kemble et al., 1994; Melikyan et al., 1997, 2000; Chernomordik et al., 1998; Armstrong et al., 2000). In two different reconstituted assays, we did not previously observe the hemifused state with full-length neuronal SNAREs (Weber et al., 1998; Fix et al., 2004). Unlike the work reported here, those two assays featured a simplified lipid and protein composition, which may have facilitated full fusion at the expense of the hemifusion endstate. This conclusion is supported by recent experiments demonstrating hemifusion when yeast SNARE proteins are reconstituted into liposomes at very low surface densities, but not at surface densities comparable to our earlier studies (Xu et al., 2005).

Herein, by monitoring lipid mixing and content mixing simultaneously in individual events, we found that (in addition to complete fusion) SNAREs promote hemifusion to a surprising degree. Fully one third of the events involved hemifusion, which could be either permanent (major outcome) or reversible (minor outcome). These hemifusion phenotypes were observed using different lipidic and soluble content markers. In addition to the diversity of fluid phase markers used in the cell–cell fusion assay, we also performed electrophysiological measurements to discern the existence of connecting pores between hemifused cells. The capacitance measurements are consistent with a description of a pore-free hemifusion diaphragm, although our current levels of sensitivity cannot rule out very small nonenlarging "micro" pores (Melikyan et al., 1995a). The conductance measurements give no indication of a dynamic pore population undergoing opening and closure within our resolution limit (∼2 nm). We were not able to capture pore formation during any complete cell–cell fusion event in these experiments. Although "stable" pores are likely to be very short lived, the cell fusion assay is limited by a long kinetic, probably

involving cell–cell contact geometries distinct from the process of SNARE pairing (Hu et al., 2003). Unfortunately, our recording period has been limited to a few minutes of patch stability. Thus, we can efficiently patch cells before or after the fusion event, but we have not yet observed a cell that fused during the relatively short lifetime of the patch. Experiments to optimize the assay for fusion pore description are ongoing in our lab.

Interestingly, replacement of the TMD of flipped SNAREs by a GPI-anchor motif produced only hemifusion as fusion outcome, highlighting its role in fusion pore opening. Because the amount of cell surface GPI-anchored SNAREs was similar to the respective flipped SNAREs, as revealed by biotinylation experiments (unpublished data), the incapability of the GPI-SNARE cells to produce full fusion is more probably due to an impairment in the transduction of the generated force during the zipping up of the SNARE proteins to fusing bilayers rather than an effect of the low cell surface concentration of SNARE proteins.

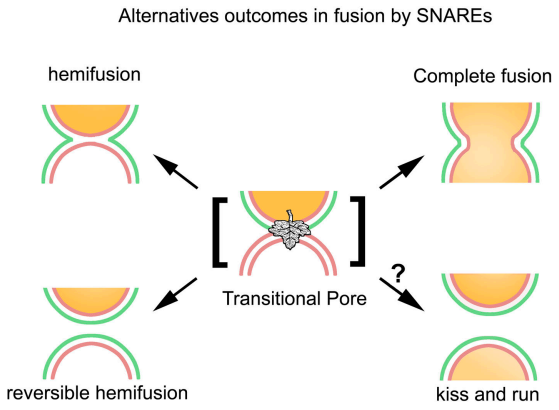

Figure 9. **Alternative outcomes of SNARE-mediated membrane fusion.** Formation of the SNARE complex leads to the formation of a transitional pore. The thermodynamic properties of the transitional pore drive membrane fusion to complete fusion, hemifusion, reversible hemifusion, or kiss and run.

Alternative outcomes can potentially be modulated for SNARE-dependent fusion

The diversity of fusion outcomes indicates a high degree of functional and conformational dynamics within the structure of the fusion pore formed by isolated SNARE proteins. For pure lipid bilayers, the activation energy required for bilayer fusion is thought to be ~40 k_BT (Kuzmin et al., 2001; Markin and Albanesi, 2002). Recent models suggest that neither mixing of the outer leaflets (hemifusion) nor mixing of the inner leaflets is the largest energetic barrier (Cohen and Melikyan, 2004). Instead, it appears that expansion of the fusion pore requires the greatest energetic input. In such a model, both hemifusion and reversible pore formation are (relatively) low energy intermediates. A simple interpretation of our results is that whereas SNAREs are intrinsically capable of full fusion, the free energy available in the pool of conformational variants only just favors such a result. This means that modest changes in free energy, which may manifest themselves in the form of different lipid compositions, different SNARE concentrations, or the binding/activation of specific regulatory proteins, could decisively tilt the balance of fusion outcomes to favor any one of the three that we observe (Fig. 9).

There are many proteins known that bind to SNAREs and which could potentially regulate the fusion pore. The n-Sec1 protein has been shown to influence the kinetic of fusion pore opening (Fisher et al., 2001). Other proteins that bind SNAREs and are intimately linked to regulated exocytosis include synaptotagmin (Bai et al., 2004), complexin (Reim et al., 2001), α-SNAP, NSF (Mayer et al., 1996), and Munc13 (Brose et al., 2000). Furthermore, the lipid composition could influence the pore structure, either by directly manipulating the SNARE conformations or by regulating the surface distribution density of active SNARE complexes (i.e., in the form of raft domains; Lang et al., 2001; Salaun et al., 2005). The molecular composition of the transitional pore is unknown. It has been proposed that the fusion pore is formed at least in part by a circular arrangement of five to eight Syntaxin transmembrane segments and that lipid molecules might intercalate between them to complete the structure (Han et al., 2004). Lipid mixing just within this pore (i.e., the formation of a stalk) has been postulated from studies with HA proteins and termed "restricted hemifusion;" however, lipid mixing itself cannot be detected in these structures, perhaps because the HA multimers or the SNARE complexes making up the pore block lipid movement out of the pore (Chernomordik et al., 1998). Similarly, hemifusion has been postulated as an explanation for the arrested fusion state of SNARE TMD mutants, which only progress to full fusion after addition of inverted cone-shaped lipids (Grote et al., 2000). Certainly, the closely related process of kiss and run in which content (or a portion thereof) is released in a transient association of vesicles with target (Klyachko and Jackson, 2002; Gandhi and Stevens, 2003) can be of prime physiological relevance in the nervous system and can be dynamically regulated (Staal et al., 2004). We suggest that this diverse physiology can result from a core fusion machinery—SNAREs—which is energetically positioned to allow alternative outcomes with a minimum of regulatory influence.

Materials and methods

Constructs and stable cell lines

To generate GPI-anchored VAMP2 (aa 2–92), DNA encoding the signal sequence of prepolactin and VAMP2 (aa 2–92) was amplified by PCR using primer EcoRSS (GTGGAATTCGCTTGTTCTTTTTGCAGAAGCTCAG) and primer VAMP92Xho (TTGGCTCGAGGTTTTTCCACCAGTATTTGCGC) with plasmid-flipped VAMP2/T27A (Hu et al., 2003) as template. The PCR product was digested with EcoRI and XhoI. The GPI motif from decay-accelerating factor was amplified by PCR from a plasmid that encodes a GPI-anchored pH-sensitive GFP mutant (Miesenbock et al., 1998) using primer GPIFor (AAACCTCGAGCCAAATAAAGGAAGTGGAACCAC) and GPIRev (AAACGGGCCCCTAAGTCAGCAAGCCCATGGTTAC). The PCR product was digested with XhoI and ApaI. Both of the enzyme-digested PCR products were cloned into the EcoRI and ApaI sites of pcDNA3.1(+) in a single ligation reaction, yielding the plasmid GPI-anchored VAMP2 (aa 2–92). GPI-anchored VAMP2 (aa 2–84), GPI-anchored flipped Syntaxin 1 (aa 186–265), and GPI-anchored Syntaxin 1 (aa 186–256) were generated in a similar manner. DNA encoding the signal sequence and VAMP2 (aa 2–84) was amplified by PCR using primer EcoRSS and primer VAMP84Xho (TTGGCTCGAGGAGCTTGGCTGCACTTGTTTC) with plasmid-flipped VAMP2/T27A as template. DNA encoding the signal sequence and Syntaxin 1 (aa 186–265) was ampli-

fied by PCR using primer EcoRSS and primer Syn265Xho (TTGGCTCGAGCTTCTTCCTGCGTGCCTTGCTC) with plasmid-flipped Syntaxin (Hu et al., 2003) as template. DNA encoding the signal sequence and Syntaxin 1 (aa 186–256) was amplified by PCR using primer EcoRSS and primer Syn256Xho (TTGGCTCGAGCTTGACGGCCTTCTTGGTGTCAG) with plasmid-flipped Syntaxin as template.

To obtain stable cell lines coexpressing flipped SNAREs or GPI-anchored cytoplasmic domains of SNAREs with appropriate fluorescent protein, different constructs detailed in the following paragraph were generated based on the pBI plasmid. This vector is a bidirectional mammalian expression vector of the Tet-Off gene expression system (Baron et al., 1995). The pBI plasmid allowed us to simultaneously regulate the expression of both the SNAREs and the fluorescent protein genes. Both genes are under the control of a single tetracycline-responsive element, which in the presence of doxycycline or tetracycline down-regulate their expression. To generate pBI-GPI-VAMP2 (2–92)-RFP-nes construct, DNA-encoding RFP-nes was amplified by PCR using primer RFP–NotI5 (GCGGCCGCGCCACCATGGCCTCCTCC) and primer RFP–SalI3 (CGTATTGTCGACCTAATCCAGCTCAAGC) with pcDNA3.1(+)RFP-nes as template (Hu et al., 2003). DNA encoding the signal sequence and GPI-VAMP2 (2–92) was amplified by PCR using primer GPIV2-MluI5 (AAGTACGCGTCGCTTGTTCTTTTTGC) and primer GPIV2-EcoRV3 (ATTGGATATCTAAGTCAGCAAGCCC) with plasmid pCDNA3.1(+)GPI-VAMP2 (2–92) as template. The PCR product was digested with MluI and EcoRV and cloned into the same sites in the pBI-RFP-nes vector. The same procedure was followed to generate the constructs pBI-GPI-VAMP2 (2–86)-RFP-nes and pBI-VAMP2 (2–116)-RFP-nes. DNA encoding the signal sequence and GPI-VAMP2 (2–86) was amplified by PCR using the same primers as GPI-VAMP2 (2–92) with plasmid pCDNA3.1(+)GPI-VAMP2 (2–86) as template. DNA encoding the signal sequence and flipped VAMP2/T27A was amplified by PCR using primer GPIV2-MluI5 and primer FlV2-EcoRV3 (AGAGATATCTTAAGTGCTGAAGTAAACG) with plasmid pCDNA3.1(+) flipped VAMP2/T27A as template. To generate pBI-GPI-Syntaxin (186–265)-flipped SNAP-25-IRES-CFP-nls, DNA encoding the signal sequence and GPI-Syntaxin (186–265) was amplified by PCR using primer GPISy–NotI5 (AATCAAGCGGCCGCTTGTTCTTTTTGC) and primer GPISy-SalI3 (GCTAATGTCGACCTAAGTCAGCAAGCCCATGG) with plasmid pCDNA3.1(+)GPI-Syntaxin (186–265) as template. The PCR product was digested with NotI and SalI and cloned into the same sites in the pBI vector. DNA encoding the signal sequence and SNAP-25 encoding the IRES sequence and CFP-nls were amplified by PCR using primer S25C-MluI5 (TATACGCGTGCCACCATGGACAGCAAAGGTTCG) and primer S25C-EcoRV3 (CGAAGATATCTTATCTAGATCCGGTGGATCCTACC) with plasmid pCH-44 as template (Hu et al., 2003). The PCR product was digested with MluI and EcoRV and cloned into the same sites in the pBI-GPI-Syntaxin (186–265) vector. pBI-GPI-Syntaxin (186–256)-flipped SNAP-25-IRES-CFP-nls and pBI-flipped Syntaxin (186–288)-flipped SNAP-25-IRES-CFP-nls were generated in a similar manner. DNA encoding the signal sequence and GPI-Syntaxin (186–256) was amplified by PCR using same primer as GPI-Syntaxin (186–265) with plasmid pCDNA3.1(+)GPI-Syntaxin (186–256) as template. DNA encoding the signal sequence and Syntaxin (186–288) was amplified by PCR using primer GPISy–NotI5 and primer FlSy-SalI3 (TAATGTCGACTATCCAAAGATGCCCC) with plasmid pCDNA3.1(+)-flipped Syntaxin (186–288) as template (Hu et al., 2003).

To generate the pAU1-GPI construct, two complementary oligonucleotides, AU1 × 2F (CCGGTCGCCACCATGGACACATACCGATACATAGACACATACCGATACATACT) and AU1 × 2R (GTACAGTATGTATCGGTATGTGTCTATGTATCGGTATGTGTCCATGGTGGCGA), encoding two repetitions of the six amino acid epitope AU1 (DTYRYI) were hybridized. After hybridization, the AgeI and BsrGI restriction sites were generated. The pEYFP-GPI plasmid (Keller and Simons, 1997) was digested with AgeI and BsrGI to release the EYFP and the remaining plasmid was purified. The double-stranded DNA fragment and the purified plasmid containing the signal sequence and the GPI motif were ligated, yielding the plasmid containing the signal sequence with the epitope AU1 fused to a GPI-anchored motif.

To generate the pHA-f construct, two complementary oligonucleotides, HAF (CCGGTGCCACCATGTACCCATATGACGTACCAGACTACGCATCACTACT) and HAR (GTACAGTAGTGATGCGTAGTCTGGTACGTCATATGGGTACATGGTGGCA), encoding the nine amino acid epitope HA (YPYDVPDYA) were hybridized. After hybridization, the AgeI and BsrGI restriction sites were generated. The pEGFP-f plasmid (CLONTECH Laboratories, Inc.), which encodes for the EGFP fused to a farnesylation signal from c-Ha-Ras, was digested with AgeI and BsrGI to release the EGFP, and the remaining plasmid was purified. The double-stranded fragment and the purified plasmid containing the farnesylation sequence were ligated, yielding the plasmid encoding the epitope HA with a farnesylation motif. All coding sequences were confirmed by DNA sequencing.

The v-SNARE set of constructs were used to generate the respective double stable Tet-Off CHO cell line; they will hereafter be referred as flipped v-cells or GPI v-cells, respectively. On the other hand, the t-SNARE set of constructs were used to generate the respective double stable MEF-3T3 Tet-Off cell line; they will hereafter be referred as flipped t-cells or GPI t-cells, respectively.

Cell–cell fusion assay

48 h before performing the assay, 3×10^4 CHO v-cells previously grown for at least 5 d in complete medium in the absence of doxycycline were seeded on sterile 12-mm glass coverslips contained in 24-well plates. MEF 3T3 t-cells previously grown for 7 d in complete medium in the absence of doxycycline were detached from the dishes with EDTA (Cell Dissociation Solution; Sigma-Aldrich). The detached cells were counted with a hemacytometer, centrifuged at 200 *g*, and resuspended in Hepes-buffered DME supplemented with 10% FCS. 3×10^4 of these t-cells were added to each coverslip already containing the v-cells. After various times at 37°C in 5% CO_2, the coverslips were gently washed once with PBS supplemented with 0.1 g/liter $CaCl_2$ and 0.1 g/liter $MgCl_2$ (PBS++), and then fixed with 4% PFA for 30 min, washed three times with PBS++, and incubated for 15 min with 1 μg/ml FITC-Cholera Toxin β-subunit (Sigma-Aldrich). After three washes with PBS++, the coverslips were mounted with Prolong Antifade Gold mounting medium (Molecular Probes). Confocal images were collected as indicated in the Image acquisition section. At each time point, the total number of fused cells (f) or hemifused cells (hf) and the total number of v-cells (V) and t-cells (T) in contact with each other (but not yet fused or hemifused) in random fields were determined. The efficiency of fusion (F) or lipid mixing (LM), as percentages, in both original flipped SNARE fusion and hemifusion assays were calculated as follows: $F = 2f/(V + T + 2f) \times 100$; $LM = 2hf/(V + T + 2hf)$.

Image acquisition

Images were acquired on a confocal microscope (model TCS SP2 AOBS; Leica) equipped with LCS software (Leica) and usually using a HCX PL APO 40×, 1.25 NA oil immersion objective. For higher magnification images, a HCX PL APO 63×, 1.4 NA oil immersion objective was used. The images were processed with Adobe Photoshop software.

Cell staining

Before performing the fusion assay, cells cotransfected with the indicated flipped or GPI-anchored SNARE and CFP-nls (as a transfection marker) were incubated with prewarmed 2 μM CMFDA, 2 μM CMTPX, 15 μM Blue CMF_2HC, or 0.5 μM Calcein AM (green or orange) in serum-free medium for 30 min at 37°C. After this time, the solution was replaced by fresh medium and cells were incubated for an additional 30 min to allow the processing of the dye, and washed three times with PBS.

Immunocytochemistry

24 h after transfection, COS-7 cells were fixed with 4% PFA in PBS++. Primary antibodies were incubated with the cells at the following dilutions: anti-Myc mAb, 1:500; anti-SNAP-25 polyclonal antibody (Synaptic Systems GmbH), 1:100; anti-GFP polyclonal antibody, 1:500; and HPC-1 anti-Syntaxin mAb, 1:1,000. Fluorophore-conjugated secondary antibodies (Jackson ImmunoResearch Laboratories) were used at dilutions of 1:500–1:1,000. For double staining, the cells were incubated first with a mixture of the primary antibodies, and then with a mixture of the secondary antibodies

Soluble t-SNARE binding assay

The t-SNARE cytoplasmic domains (with no internal cysteines and containing his6-SNAP-25 and Syntaxin1A [residues 1-265-L-C]) were expressed in *Escherichia coli* as described previously (McNew et al., 2000b). COS-7 cells were transfected with flipped VAMP2/T27A-IRES2-EGFP or EGFP (as control). 24 h after transfection, the cells were incubated with 5 μM of soluble t-SNARE complex in Hepes-buffered DME (high glucose; GIBCO BRL) with 10% FBS in the presence of 0.5 mM DTT. After 1 h at 37°C in 5% CO_2, the cells were washed four times with the DME medium, washed once with PBS++, and fixed with 4% PFA. Surface-bound t-SNARE was detected with HPC-1 anti-Syntaxin antibody.

Membrane capacitance measurements

Solutions used for patch clamp recordings were as follows. The bath saline contained PBS. Patch pipette solution contained 139 mM gluconic acid, 2 mM $MgCl_2$, 0.1 mM $CaCl_2$, 10 mM Hepes, pH 7.4, 1 mM EGTA,

1 mM ATP, and 2 mM GTP. Whole cell perforated patches were obtained by using 100 μg/ml nystatin in the patch pipette as previously described (Horn and Marty, 1988). Whole cell capacitance and resistance measurements were performed on single CHO cells or 3T3 fibroblasts, or hemifused CHO-3T3 cells by patching either the CHO or the 3T3 cell. The current was filtered using a 4-pole, 5-kHz Bessel filter built into an Axopatch 200B amplifier (Axon Instruments, Inc.) and sampled at 20 kHz (PCI-6052E; National Instruments). For the membrane resistance recordings in the whole cell configuration, this yielded essentially no time distortion for events with durations >200 μs while broadening events of shorter duration toward this value. Data files were saved in Igor binary format for further analysis using a locally written routine in Igor Pro (Wavemetrics).

For capacitance measurements, a perforated cell was kept at −60 mV holding potential, whereas square +5 mV steps (V_0) were applied at 20 Hz frequency; the resolution of these measurements was therefore 100 ms. Cell capacitance was estimated by fitting the current transient with an exponential function as described in Lindau and Neher (1988). In brief, the current through the whole cell circuit after application of a square voltage pulse consists of an initial transient (I_0) that decays to a steady-state value (I_{ss}) with an exponential time constant (τ). Cell electrical characteristics are calculated using the following equations:

$$R_a = \frac{V_0}{I_0};$$

$$R_m = \frac{V_0}{I_{ss} - R_a};$$

$$Cm = \tau\left(\frac{1}{R_a} + \frac{1}{R_m}\right).$$

Where R_a is access resistance and R_m and C_m are the resistance and the capacitance of the cell membrane, correspondingly.

For the whole cell resistance measurements, the current through the cell membrane was determined in the absence of voltage pulses providing a resolution of 100 μs. The cell was kept at a constant −60 mV holding potential (V_{hold}) and assuming that R_a was much smaller than R_m, the latter was estimated as

$$R_{m'} = \frac{V_{hold}}{I_{ss}},$$

where $R_{m'}$ is the resistance of the cell at −60 mV and I_{ss} is the whole cell current. If two hemifused cells formed a conducting fusion pore (Fig. 8 B), the current would depend on its resistance (R_p) according to the relationship:

$$I_{ss}(2cells) = \frac{V_{hold}}{R_{total}};$$

$$R_{total} = \frac{R_{m1} \times (R_{m2} + R_p)}{(R_{m1} + R_{m2} + R_p)},$$

where R_{m1} and R_{m2} equal the resistance of cells 1 and 2, respectively. Note that when R_p equals zero, the resulting current is twofold higher than that of a single cell, whereas when R_p increases, the change in I_{ss} becomes gradually smaller.

We thank Dr. F. Paumet for comments on the manuscript.

This work was supported by a grant from the National Institutes of Health (J.E. Rothman).

Submitted: 19 January 2005
Accepted: 10 June 2005

References

Albillos, A., G. Dernick, H. Horstmann, W. Almers, G. Alvarez de Toledo, and M. Lindau. 1997. The exocytotic event in chromaffin cells revealed by patch amperometry. *Nature.* 389:509–512.

Alvarez de Toledo, G., R. Fernandez-Chacon, and J.M. Fernandez. 1993. Release of secretory products during transient vesicle fusion. *Nature.* 363:554–558.

Armstrong, R.T., A.S. Kushnir, and J.M. White. 2000. The transmembrane domain of influenza hemagglutinin exhibits a stringent length requirement to support the hemifusion to fusion transition. *J. Cell Biol.* 151:425–437.

Bai, J., C.T. Wang, D.A. Richards, M.B. Jackson, and E.R. Chapman. 2004. Fusion pore dynamics are regulated by synaptotagmin*t-SNARE interactions. *Neuron.* 41:929–942.

Baron, U., S. Freundlieb, M. Gossen, and H. Bujard. 1995. Co-regulation of two gene activities by tetracycline via a bidirectional promoter. *Nucleic Acids Res.* 23:3605–3606.

Breckenridge, L.J., and W. Almers. 1987. Currents through the fusion pore that forms during exocytosis of a secretory vesicle. *Nature.* 328:814–817.

Brose, N., C. Rosenmund, and J. Rettig. 2000. Regulation of transmitter release by Unc-13 and its homologues. *Curr. Opin. Neurobiol.* 10:303–311.

Chernomordik, L.V., G.B. Melikyan, and Y.A. Chizmadzhev. 1987. Biomembrane fusion: a new concept derived from model studies using two interacting planar lipid bilayers. *Biochim. Biophys. Acta.* 906:309–352.

Chernomordik, L.V., V.A. Frolov, E. Leikina, P. Bronk, and J. Zimmerberg. 1998. The pathway of membrane fusion catalyzed by influenza hemagglutinin: restriction of lipids, hemifusion, and lipidic fusion pore formation. *J. Cell Biol.* 140:1369–1382.

Cohen, F.S., and G.B. Melikyan. 1998. Methodologies in the study of cell-cell fusion. *Methods.* 16:215–226.

Cohen, F.S., and G.B. Melikyan. 2004. The energetics of membrane fusion from binding, through hemifusion, pore formation, and pore enlargement. *J. Membr. Biol.* 199:1–14.

Fisher, R.J., J. Pevsner, and R.D. Burgoyne. 2001. Control of fusion pore dynamics during exocytosis by Munc18. *Science.* 291:875–878.

Fix, M., T.J. Melia, J.K. Jaiswal, J.Z. Rappoport, D. You, T.H. Sollner, J.E. Rothman, and S.M. Simon. 2004. Imaging single membrane fusion events mediated by SNARE proteins. *Proc. Natl. Acad. Sci. USA.* 101:7311–7316.

Gandhi, S.P., and C.F. Stevens. 2003. Three modes of synaptic vesicular recycling revealed by single-vesicle imaging. *Nature.* 423:607–613.

Grote, E., M. Baba, Y. Ohsumi, and P.J. Novick. 2000. Geranylgeranylated SNAREs are dominant inhibitors of membrane fusion. *J. Cell Biol.* 151:453–466.

Han, X., C.T. Wang, J. Bai, E.R. Chapman, and M.B. Jackson. 2004. Transmembrane segments of syntaxin line the fusion pore of Ca^{2+}-triggered exocytosis. *Science.* 304:289–292.

Hille, B. 1984. Ion Channels of Excitable Membranes. Sinauer Associates Inc., Sunderland, MA. 514 pp.

Horn, R., and A. Marty. 1988. Muscarinic activation of ionic currents measured by a new whole-cell recording method. *J. Gen. Physiol.* 92:145–159.

Hu, C., M. Ahmed, T.J. Melia, T.H. Sollner, T. Mayer, and J.E. Rothman. 2003. Fusion of cells by flipped SNAREs. *Science.* 300:1745–1749.

Keller, P., and K. Simons. 1997. Post-Golgi biosynthetic trafficking. *J. Cell Sci.* 110:3001–3009.

Kemble, G.W., T. Danieli, and J.M. White. 1994. Lipid-anchored influenza hemagglutinin promotes hemifusion, not complete fusion. *Cell.* 76:383–391.

Klyachko, V.A., and M.B. Jackson. 2002. Capacitance steps and fusion pores of small and large-dense-core vesicles in nerve terminals. *Nature.* 418:89–92.

Kuzmin, P.I., J. Zimmerberg, Y.A. Chizmadzhev, and F.S. Cohen. 2001. A quantitative model for membrane fusion based on low-energy intermediates. *Proc. Natl. Acad. Sci. USA.* 98:7235–7240.

Kweon, D.H., C.S. Kim, and Y.K. Shin. 2003. Regulation of neuronal SNARE assembly by the membrane. *Nat. Struct. Biol.* 10:440–447.

Lang, T., D. Bruns, D. Wenzel, D. Riedel, P. Holroyd, C. Thiele, and R. Jahn. 2001. SNAREs are concentrated in cholesterol-dependent clusters that define docking and fusion sites for exocytosis. *EMBO J.* 20:2202–2213.

Lee, J., and B.R. Lentz. 1997. Outer leaflet-packing defects promote poly(ethylene glycol)-mediated fusion of large unilamellar vesicles. *Biochemistry.* 36:421–431.

Lindau, M., and E. Neher. 1988. Patch-clamp techniques for time-resolved capacitance measurements in single cells. *Pflügers Arch.* 411:137–146.

Lindau, M., and W. Almers. 1995. Structure and function of fusion pores in exocytosis and ectoplasmic membrane fusion. *Curr. Opin. Cell Biol.* 7:509–517.

Markin, V.S., and J.P. Albanesi. 2002. Membrane fusion: stalk model revisited. *Biophys. J.* 82:693–712.

Mayer, A., W. Wickner, and A. Haas. 1996. Sec18p (NSF)-driven release of Sec17p (alpha-SNAP) can precede docking and fusion of yeast vacuoles. *Cell.* 85:83–94.

McNew, J.A., F. Parlati, R. Fukuda, R.J. Johnston, K. Paz, F. Paumet, T.H. Sollner, and J.E. Rothman. 2000a. Compartmental specificity of cellular membrane fusion encoded in SNARE proteins. *Nature.* 407:153–159.

McNew, J.A., T. Weber, F. Parlati, R.J. Johnston, T.J. Melia, T.H. Sollner, and J.E. Rothman. 2000b. Close is not enough: SNARE-dependent membrane fusion requires an active mechanism that transduces force to membrane anchors. *J. Cell Biol.* 150:105–117.

Melia, T.J., T. Weber, J.A. McNew, L.E. Fisher, R.J. Johnston, F. Parlati, L.K. Mahal, T.H. Sollner, and J.E. Rothman. 2002. Regulation of membrane fusion by the membrane-proximal coil of the t-SNARE during zippering of SNAREpins. *J. Cell Biol.* 158:929–940.

Melikyan, G.B., W.D. Niles, V.A. Ratinov, M. Karhanek, J. Zimmerberg, and F.S. Cohen. 1995a. Comparison of transient and successful fusion pores connecting influenza hemagglutinin expressing cells to planar membranes. *J. Gen. Physiol.* 106:803–819.

Melikyan, G.B., J.M. White, and F.S. Cohen. 1995b. GPI-anchored influenza hemagglutinin induces hemifusion to both red blood cell and planar bilayer membranes. *J. Cell Biol.* 131:679–691.

Melikyan, G.B., S.A. Brener, D.C. Ok, and F.S. Cohen. 1997. Inner but not outer membrane leaflets control the transition from glycosylphosphatidylinositol-anchored influenza hemagglutinin-induced hemifusion to full fusion. *J. Cell Biol.* 136:995–1005.

Melikyan, G.B., R.M. Markosyan, M.G. Roth, and F.S. Cohen. 2000. A point mutation in the transmembrane domain of the hemagglutinin of influenza virus stabilizes a hemifusion intermediate that can transit to fusion. *Mol. Biol. Cell.* 11:3765–3775.

Miesenbock, G., D.A. De Angelis, and J.E. Rothman. 1998. Visualizing secretion and synaptic transmission with pH-sensitive green fluorescent proteins. *Nature.* 394:192–195.

Monck, J.R., and J.M. Fernandez. 1992. The exocytotic fusion pore. *J. Cell Biol.* 119:1395–1404.

Parlati, F., O. Varlamov, K. Paz, J.A. McNew, D. Hurtado, T.H. Sollner, and J.E. Rothman. 2002. Distinct SNARE complexes mediating membrane fusion in Golgi transport based on combinatorial specificity. *Proc. Natl. Acad. Sci. USA.* 99:5424–5429.

Paumet, F., B. Brugger, F. Parlati, J.A. McNew, T.H. Sollner, and J.E. Rothman. 2001. A t-SNARE of the endocytic pathway must be activated for fusion. *J. Cell Biol.* 155:961–968.

Paumet, F., V. Rahimian, and J.E. Rothman. 2004. The specificity of SNARE-dependent fusion is encoded in the SNARE motif. *Proc. Natl. Acad. Sci. USA.* 101:3376–3380.

Razinkov, V.I., G.B. Melikyan, and F.S. Cohen. 1999. Hemifusion between cells expressing hemagglutinin of influenza virus and planar membranes can precede the formation of fusion pores that subsequently fully enlarge. *Biophys. J.* 77:3144–3151.

Reim, K., M. Mansour, F. Varoqueaux, H.T. McMahon, T.C. Sudhof, N. Brose, and C. Rosenmund. 2001. Complexins regulate a late step in Ca^{2+}-dependent neurotransmitter release. *Cell.* 104:71–81.

Rohde, J., L. Dietrich, D. Langosch, and C. Ungermann. 2003. The transmembrane domain of Vam3 affects the composition of cis- and trans-SNARE complexes to promote homotypic vacuole fusion. *J. Biol. Chem.* 278:1656–1662.

Rosales Fritz, V.M., J.L. Daniotti, and H.J.F. Maccioni. 1997. Chinese hamster ovary cells lacking GM1 and GD1a synthesize gangliosides upon transfection with human GM2 synthase. *Biochim. Biophys. Acta.* 1354:153–158.

Salaun, C., G.W. Gould, and L.H. Chamberlain. 2005. The SNARE proteins SNAP-25 and SNAP-23 display different affinities for lipid rafts in PC12 cells. Regulation by distinct cysteine-rich domains. *J. Biol. Chem.* 280:1236–1240.

Sollner, T., S.W. Whiteheart, M. Brunner, H. Erdjument-Bromage, S. Geromanos, P. Tempst, and J.E. Rothman. 1993. SNAP receptors implicated in vesicle targeting and fusion. *Nature.* 362:318–324.

Staal, R.G., E.V. Mosharov, and D. Sulzer. 2004. Dopamine neurons release transmitter via a flickering fusion pore. *Nat. Neurosci.* 7:341–346.

Sutton, R.B., D. Fasshauer, R. Jahn, and A.T. Brunger. 1998. Crystal structure of a SNARE complex involved in synaptic exocytosis at 2.4 A resolution. *Nature.* 395:347–353.

Tamm, L.K., J. Crane, and V. Kiessling. 2003. Membrane fusion: a structural perspective on the interplay of lipids and proteins. *Curr. Opin. Struct. Biol.* 13:453–466.

Weber, T., B.V. Zemelman, J.A. McNew, B. Westermann, M. Gmachl, F. Parlati, T.H. Sollner, and J.E. Rothman. 1998. SNAREpins: minimal machinery for membrane fusion. *Cell.* 92:759–772.

Xu, Y., F. Zhang, Z. Su, J.A. McNew, and Y.K. Shin. 2005. Hemifusion in SNARE-mediated membrane fusion. *Nat. Struct. Mol. Biol.* 12:417–422.

Zimmerberg, J., R. Blumenthal, D.P. Sarkar, M. Curran, and S.J. Morris. 1994. Restricted movement of lipid and aqueous dyes through pores formed by influenza hemagglutinin during cell fusion. *J. Cell Biol.* 127:1885–1894.